ISSN 1674-1056
http://cpb.iphy.ac.cn
http://iopscience.iop.org/cpb
中国物理 B
Chinese Physics
中国物理
Chinese Physics B

Real-space parallel density matrix renormalization group with adaptive boundaries

Fu-Zhou Chen(陈富州), Chen Cheng(程晨), and Hong-Gang Luo(罗洪刚)
Citation: Chin. Phys. B, 2021, 30 (**8**): 080202. DOI: 10.1088/1674-1056/abeb08
Journal homepage: http://cpb.iphy.ac.cn; http://iopscience.iop.org/cpb

What follows is a list of articles you may be interested in

Delta-Davidson method for interior eigenproblem in many-spin systems

Haoyu Guan(关浩宇) and Wenxian Zhang(张文献)
Chin. Phys. B, 2021, 30 (**3**): 030205. DOI: 10.1088/1674-1056/abd74a

A local refinement purely meshless scheme for time fractional nonlinear Schrödinger equation in irregular geometry region

Tao Jiang(蒋涛), Rong-Rong Jiang(蒋戎戎), Jin-Jing Huang(黄金晶), Jiu Ding(丁玖), and Jin-Lian Ren(任金莲)
Chin. Phys. B, 2021, 30 (**2**): 020202. DOI: 10.1088/1674-1056/abc0e0

Modes decomposition in particle-in-cell software CEMPIC

Aiping Fang(方爱平)†, Shanshan Liang(梁闪闪), Yongdong Li(李永东), Hongguang Wang(王洪广), and Yue Wang(王玥)
Chin. Phys. B, 2020, 29 (**10**): 100205. DOI: 10.1088/1674-1056/abaed6

Improved hybrid parallel strategy for density matrix renormalization group method

Fu-Zhou Chen(陈富州), Chen Cheng(程晨), Hong-Gang Luo(罗洪刚)
Chin. Phys. B, 2020, 29 (**7**): 070202. DOI: 10.1088/1674-1056/ab8a42

Finite-difference time-domain modeling of curved material interfaces by using boundary condition equations method

Jia Lu(卢佳), Huaichun Zhou(周怀春)
Chin. Phys. B, 2016, 25 (**9**): 090203. DOI: 10.1088/1674-1056/25/9/090203

Real-space parallel density matrix renormalization group with adaptive boundaries*

Fu-Zhou Chen(陈富州)[1], Chen Cheng(程晨)[1], and Hong-Gang Luo(罗洪刚)[1,2,†]

[1] School of Physical Science and Technology, Lanzhou University, Lanzhou 730000, China
[2] Beijing Computational Science Research Center, Beijing 100084, China

(Received 30 November 2020; revised manuscript received 10 February 2021; accepted manuscript online 2 March 2021)

We propose an improved real-space parallel strategy for the density matrix renormalization group (DMRG) method, where boundaries of separate regions are adaptively distributed during DMRG sweeps. Our scheme greatly improves the parallel efficiency with shorter waiting time between two adjacent tasks, compared with the original real-space parallel DMRG with fixed boundaries. We implement our new strategy based on the message passing interface (MPI), and dynamically control the number of kept states according to the truncation error in each DMRG step. We study the performance of the new parallel strategy by calculating the ground state of a spin-cluster chain and a quantum chemical Hamiltonian of the water molecule. The maximum parallel efficiencies for these two models are 91% and 76% in 4 nodes, which are much higher than the real-space parallel DMRG with fixed boundaries.

Keywords: density matrix renormalization group, strongly correlated systems, message passing interface

PACS: 02.70.–c, 71.10.Fd, 71.27.+a, 05.10.Cc **DOI:** 10.1088/1674-1056/abeb08

1. Introduction

The density matrix renormalization group (DMRG) method was originally proposed to calculate ground states of one-dimensional strongly correlated systems with high precision.[1,2] Nowadays, DMRG has been considered as a variationally optimizing algorithm of the matrix product state (MPS),[3,4] and researchers have extended its applications to one-dimensional systems with long-range interactions,[5–8] quasi-two-dimensional lattice models[9–11] and even some two-dimensional lattices.[12,13,15–17] Other than calculations based on the real space representations, methods in momentum space[18] and hybrid-real-momentum-space[19,20] are developed to challenge two-dimensional electronic systems. In addition, DMRG for quantum chemical Hamiltonians is also a very important tool to get highly accurate ground states of small molecules and transition metal clusters.[21–24] In these extended applications, due to large entanglement entropy between subsystems, a large number of kept states and dozens of sweeps are usually necessary to get a converged DMRG result with moderate accuracy. This can result in huge memory cost and extremely long computational time, and optimizations of the numerical method becomes more and more important.

In practice, there are two main approaches to accelerate the calculation. On the one hand, one can reduce the computational and storage complexities by various ways, such as symmetries of Hamiltonians, or a good initial wave function for diagonalizing the Hamiltonian in each DMRG step.[25–32] On the other hand, many parallel strategies have been proposed to take full advantages of high performance computers. For the latter, one usually divides calculations in each DMRG step to several parts, and then takes corresponding computations parallelly. For example, in a DMRG step, calculations can be distributed according to good quantum numbers,[33] or different terms in the Hamiltonian.[34] This parallel scheme has been applied to implementations on the shared memory, the distributed memory and the hybrid architecture with both central processing units (CPUs) and graphics processing units (GPUs).[33–38] In another parallel strategy, the so-called real-space parallel DMRG,[39] DMRG steps are distributed based on the real-space index of the local tensor to be optimized in an MPS. Different from previous strategies, the lattice is partitioned into several regions, and DMRG sweeps on these regions can be performed in parallel. This method is independent of specific systems, and can easily cooperate with other parallel strategies. It greatly benefits to studies of two-dimensional lattice models which are difficult to get high performance in the distributed memory computers. In the pioneer work of Stoudenmire and White,[39] it was reported that nearly ideal speedup can be obtained in solving the ground state of the pure Q_2 model on the square lattice and the Heisenberg model on the triangular lattice. Recently, this real-space parallel strategy has also been developed to accelerate algorithms generalized from DMRG, for example, the real-space parallel infinite-system DMRG,[40] parallel implementation of the time-evolving block decimation algorithm,[41] and the parallel time-depedent variational principle algorithm.[42]

*Project supported by the National Natural Science Foundation of China (Grant Nos. 11674139, 11834005, and 11904145) and the Program for Changjiang Scholars and Innovative Research Team in Universities, China (Grant No. IRT-16R35).

†Corresponding author. E-mail: luohg@lzu.edu.cn

In the real-space parallel DMRG, sites are divided to several regions in advance, and each computing node takes care of DMRG sweeps within a fixed region. Synchronizations and communications are required at boundaries between these regions. In general, one can distribute regions by experience and may get fine parallel efficiency. However, it is practically impossible to ensure two neighboring tasks arriving at their shared bond simultaneously for various models and parameters. Especially, it is quite common to fix the truncation error and dynamically adjust the DMRG kept states,[28,29] which results in different computational cost for different DMRG steps at different sites and DMRG sweeps. If the system is non-uniform, the proper DMRG kept states is impractical to be predicted. All these uncertain factors make it hard to well estimate the time cost ratio of each DMRG step before DMRG calculations. Therefore, in our new strategy, we adaptively control boundaries between regions in each DMRG sweep, so that the waiting time between any two neighboring nodes is minimized. We apply our parallel scheme to calculate the ground state of a 2-leg spin-cluster chain and a quantum chemical Hamiltonian of the water molecule. In both the cases, parallel efficiency is greatly improved with adaptive boundaries.

The paper is organized as follows. First, two lattice models are introduced in Section 2, which are used to test the performance of our parallel strategy. Then we give a short review of the original real-space parallel DMRG in Section 3. Our real-space parallel strategy and some implementation details are shown in Section 4. In Section 5, we test performances of real-space parallel methods with different partitionings of lattices. The conclusion is given in Section 6.

2. The benchmark models

In this work, we adopt two model Hamiltonians to benchmark the performance of our parallel algorithm. First, we apply it to a spin-1/2 model on a clustered 2-leg ladder. This model is proposed to describe the quasi-one-dimensional material $K_2Cu_3O(SO_4)_3$,[43] where the Haldane state is observed experimentally.[44] This kind of spin-cluster chain (SCC) has attracted recent researches about quantum phase transitions and magnetic properties, both theoretically and experimentally.[45–47] The quasi-one-dimensional $K_2Cu_3O(SO_4)_3$ material can be described by the Hamiltonian[44]

$$\hat{H}_{\rm SCC} = \sum_k \hat{H}^k_{\rm intra} + \sum_k \hat{H}^k_{\rm inter}, \tag{1}$$

with intra- and inter-cluster terms

$$\begin{aligned}\hat{H}^k_{\rm intra} &= J_1 \sum_{j=1}^{n_{\rm c}} \boldsymbol{S}^{(k)}_{1,q}\boldsymbol{S}^{(k)}_{2,q} \\ &\quad + J_2 \sum_{q=1}^{n_{\rm c}-1} \left(\boldsymbol{S}^{(k)}_{1,q}\boldsymbol{S}^{(k)}_{1,q+1} + \boldsymbol{S}^{(k)}_{2,q}\boldsymbol{S}^{(k)}_{2,q+1}\right) \\ &\quad + J_3 \sum_{q=1}^{n_{\rm c}-1} \left(\boldsymbol{S}^{(k)}_{1,q}\boldsymbol{S}^{(k)}_{2,q+1} + \boldsymbol{S}^{(k)}_{2,q}\boldsymbol{S}^{(k)}_{1,q+1}\right), \\ \hat{H}^k_{\rm inter} &= J_{\rm inter} \sum_k \left(\boldsymbol{S}^{(k)}_{1,n_{\rm c}}\boldsymbol{S}^{(k+1)}_{1,1} + \boldsymbol{S}^{(k)}_{2,n_{\rm c}}\boldsymbol{S}^{(k+1)}_{2,1}\right).\end{aligned}$$

Here $\boldsymbol{S}^{(k)}_{p,q}$ is the spin-1/2 operator on the (p,q) site of kth cluster, with p (q) being the leg (rung) index. There are $2n_{\rm c}$ sites in each cluster, where $n_{\rm c}$ is the cluster length. Within a cluster, J_1 (J_2) is the nearest-neighbor interaction strength on rungs (legs), and J_3 denotes the next nearest-neighbor interaction. Between clusters, the coupling strength is determined by $J_{\rm inter}$. In this work, we set $J_{\rm inter} = 1$ as the energy unit, and fix $J_1 = J_2 = J_3 = 1$ in our calculations.

Second, we apply our parallel scheme to the quantum chemical problem. In past 2 decades, DMRG for *ab initio* quantum chemistry (QCDMRG) has been used to investigate some small molecules,[48] quasi-one-dimensional molecules,[49] transition metal complexes and clusters,[50,51] and even some molecules with heavy elements.[52] The general form of an electronic Hamiltonian in quantum chemistry is written as

$$\begin{aligned}\hat{H}_{\rm QC} &= \sum_{mn,\sigma} t_{mn}\hat{c}^\dagger_{m\sigma}\hat{c}_{n\sigma} \\ &\quad + \frac{1}{2}\sum_{mnpq,\sigma\sigma'} v_{mnqp}\hat{c}^\dagger_{m\sigma}\hat{c}^\dagger_{n\sigma'}\hat{c}_{p\sigma'}\hat{c}_{q\sigma},\end{aligned} \tag{2}$$

where m, n, p and q are indices of molecular orbitals, t_{mn} and v_{mnqp} are the one- and two-electron integrals, respectively; $\hat{c}^\dagger_{m\sigma}$ ($\hat{c}_{m\sigma}$) creates (annihilates) an electron with spin $\sigma \in \{\uparrow,\downarrow\}$ on orbital m. Here, we apply DMRG to solve the ground energy of the water molecule, with H–O bond length 0.96 Å and the H–O–H bond angle 104.5°. Molecular orbitals and electron integrals are obtained from the Hartree–Fock (HF) calculation with the cc-pcVTZ basis in PSI4.[53] This Hamiltonian can be regarded as a lattice model by considering each molecular orbital as one site.

3. Real-space parallel DMRG with fixed boundaries

In the DMRG method, the lattice is mapped to a one-dimensional chain, and the converged ground-state is finally obtained by back and forth optimizing sweeps. In the two-site DMRG algorithm, the whole Hamiltonian is expressed in four-block basis $|\alpha_{i-1}\rangle^l|\sigma_i\rangle|\sigma_{i+1}\rangle|\alpha_{i+1}\rangle^r$, where σ_i is the basis on site i and $|\alpha_{i-1}\rangle^l|\sigma_i\rangle$ ($|\sigma_{i+1}\rangle|\alpha_{i+1}\rangle^r$) is usually considered as the basis of the system (environment) block [see Fig. 1(a)]. Without loss of generality, in the following we introduce one DMRG step in a sweep from left to right, which is about to optimize the system block. First, by diagonalizing the Hamiltonian one obtains the ground-state energy $E_{\rm g}$ and wavefunction

$$|\Psi^{i,i+1}\rangle = \sum_{\alpha_{i-1}\sigma_i\sigma_{i+1}\alpha_{i+1}} \psi^{\sigma_i\sigma_{i+1}}_{\alpha_{i-1}\alpha_{i+1}}|\alpha_{i-1}\rangle^l|\sigma_i\rangle|\sigma_{i+1}\rangle|\alpha_{i+1}\rangle^r. \tag{3}$$

Then a singular value decomposition (SVD) on this eigenvector is performed as

$$\psi^{\sigma_i\sigma_{i+1}}_{\alpha_{i-1}\alpha_{i+1}} = \sum_{\alpha_i} U^i{}_{\alpha_{i-1}\sigma_i,\alpha_i} \Lambda^i{}_{\alpha_i} V^{i\dagger}{}_{\alpha_i,\alpha_{i+1}\sigma_{i+1}}, \tag{4}$$

where $\Lambda^i{}_{\alpha_i}$ are the singular values, and columns of U^i and V^i are the left and right singular vectors at the bond i, respectively. Finally, the basis of the system block is optimized via

$$|\alpha_i\rangle^l = \sum_{\alpha_{i-1}\sigma_i} U^i{}_{\alpha_{i-1}\sigma_i,\alpha_i} |\alpha_{i-1}\rangle^l |\sigma_i\rangle. \tag{5}$$

Here we keep only $|\alpha_i\rangle^l$ corresponding to the largest D singular values, as to keep a manageable dimension of the truncated Hilbert space. The truncation error of this DMRG step is $\varepsilon = 1 - \sum_{k<D} \Lambda^{i2}_k$. A full DMRG sweep contains repeating DMRG steps from left to right and back. In particular, in a DMRG step from right to left, the truncated states is calculated by

$$|\alpha_i\rangle^r = \sum_{\alpha_{i+1}\sigma_i} V^i{}_{\alpha_i,\alpha_{i+1}\sigma_{i+1}} |\sigma_{i+1}\rangle |\alpha_{i+1}\rangle^r. \tag{6}$$

In each DMRG step, the most time-consuming operation is the calculation of E_g by numerical diagonalization methods. To reduce the number of iterations in these methods, one can use a good initial wave function (as Ref. [27]) by transforming the wave function of the previous DMRG step.

In the real-space parallel DMRG, an initial partitioning is set to divide the lattice into several regions, and the size of each region is fixed for all parallel sweeps. In contrast with the real-space serial DMRG, in the real-space parallel strategy, sweeps are performed on these regions in parallel. Taking the 2-node case as an example, we review the real-space parallel algorithm in Fig. 1(b). At the shared bond connecting the two parallel regions, node 0 starts a serial DMRG sweep from right to left and optimizes enlarging right blocks. Meanwhile, node 1 carries another serial DMRG sweep from left to right and optimizes enlarging left blocks. Note that there is a sweeping direction reversing at the end of the lattice for each node, just as the serial DMRG algorithm. When sweeps on 2 nodes both reach the shared bond again from the opposite direction, we have a superblock with the updated basis $|\tilde{\alpha}_{i-1}\rangle^l |\sigma_i\rangle |\sigma_{i+1}\rangle |\tilde{\alpha}_{i+1}\rangle^r$, where $|\tilde{\alpha}_{i-1}\rangle^l$ ($|\tilde{\alpha}_{i+1}\rangle^r$) is the updated left (right) block on node 0 (1). Then optimized information is collected from both nodes and a globally optimized ground-state is retrieved by diagonalizing the Hamiltonian on the superblock. Next, we can optimize the system block on each node according to Eqs. (5) and (6), and start next parallel sweeps.

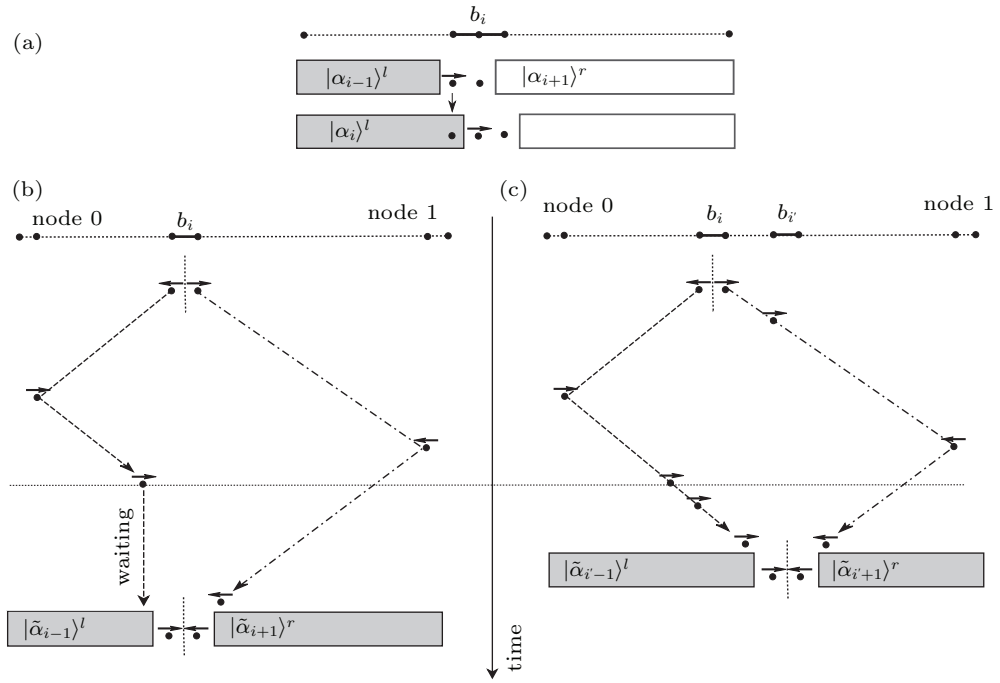

Fig. 1. (a) One DMRG step of the sweep from left to right. The chain is shown with site 1 to L, and bond b_i connects site i and $i+1$. Here $|\alpha_{i-1}\rangle^l$ are the kept states on the block containing site 1 to $i-1$, and $|\alpha_{i+1}\rangle^r$ are the kept states on the block containing site $i+2$ to L. The wave function on 4 subsystems is optimized, and the kept states $|\alpha_i\rangle^l$ are calculated for the left block of bond b_i, then next DMRG step starts. To simplify the following diagrams (b) and (c), we only show the site to be added and an arrow on it representing the sweep direction for each DMRG step. (b) One sweep of the parallel strategy with fixed boundaries in 2 nodes. The DMRG steps are performed along the dashed and dot-dashed lines with an arrow in node 0 and node 1, respectively. The first half-sweep in node 0 and node 1 starts from shared bond b_i until two nodes arrive at the left and right boundaries of the lattice, respectively, then starts the second half-sweep. Here we assume that node 0 arrives at the shared bond first, and it will wait for its neighboring node. Then the wave function is optimized on the shared bond, and both the states on the left and right block are kept. A new parallel sweep may start from this shared bond. (c) One sweep of the parallel strategy with dynamical boundaries in 2 nodes. It is the same as the original real-space parallel DMRG before node 0 arriving the shared bond. However, two nodes continue their sweeps until they arrive at a new shared bond $b_{i'}$. Therefore, there is almost no waiting time in our new strategy. After the DMRG step on shared bond $b_{i'}$, a new parallel sweep starts from this bond.

Similar to the serial DMRG, the diagonalization of the Hamiltonian on the shared bond can also be accelerated by a good initial wavefunction. Consider that the last DMRG steps before two parallel sweeps meet each other, we have the transformed wavefunctions

$$|\tilde{\Psi}^{i}\rangle = \sum_{\tilde{\alpha}_{i-1}\sigma_i\alpha_i} \tilde{\psi}^{\sigma_i}_{\tilde{\alpha}_{i-1}\alpha_i} |\tilde{\alpha}_{i-1}\rangle^{l} |\sigma_i\rangle |\alpha_i\rangle^{r}, \tag{7}$$

$$|\tilde{\Psi}^{i+1}\rangle = \sum_{\alpha_i\sigma_{i+1}\tilde{\alpha}_{i+1}} \tilde{\psi}^{\sigma_{i+1}}_{\alpha_i\tilde{\alpha}_{i+1}} |\alpha_i\rangle^{l} |\sigma_{i+1}\rangle |\tilde{\alpha}_{i+1}\rangle^{r} \tag{8}$$

from nodes 0 and 1, respectively. Here wavefunctions are expressed in 3 blocks since the *system* block is already updated using Eqs. (5) and (6). The guessing solution of the superblock is $|\Phi^{i,i+1}\rangle$ with its coefficients

$$\phi^{\sigma_i\sigma_{i+1}}_{\tilde{\alpha}_{i-1}\tilde{\alpha}_{i+1}} = \sum_{\alpha_i} \tilde{\psi}^{\sigma_i}_{\tilde{\alpha}_{i-1}\alpha_i} (\Lambda^{i}{}_{\alpha_i})^{-1} \tilde{\psi}^{\sigma_{i+1}}_{\alpha_i\tilde{\alpha}_{i+1}}, \tag{9}$$

where $\Lambda^{i}{}_{\alpha_i}$ is the singular value at b_i from the previous sweep.

In the real-space parallel DMRG scheme, there is only data communications between two neighboring nodes in calculations at their shared bond. The time cost of communications is usually a tiny proportion compared to a whole DMRG sweep, especially for large parallel regions or large number of kept states. Therefore, this parallel strategy may greatly accelerate DMRG calculations on modern high performance computers based on the distributed memory architecture. On the other hand, it can freely collaborate with other parallel algorithms on shared memory systems. The parallel efficiency of the method sensitively depends on *a priori* partitioning of real-space parallel regions. In the case of the ideal initial partitioning, each node takes comparative computations, and reaches shared bonds at almost the same time. However, in practice, it is not always easy to distribute real-space parallel regions in a good way before DMRG calculations, for various problems, models and parameters. In that case, one node may reach the shared bond and then waits for its neighbor for a long time, as shown in Fig. 1(b). Region partitioning is harder for larger number of parallel nodes. This problem can greatly affect the parallel efficiency.

4. Real-space parallel DMRG with dynamic boundaries

4.1. Algorithm

To improve the parallel efficiency for general applications, we propose a dynamical real-space parallel DMRG strategy, in which parallel regions are partitioned adaptively and therefore greatly reduce load imbalance between nodes. In our improved parallel scheme, the DMRG chain is partitioned to several regions manually for the first half-sweep, then positions of shared bonds are adjusted dynamically in latter sweeps. Here we show one sweep of the strategy in Fig. 1(c), taking 2 parallel regions as an example. In the beginning stage, two nodes begin parallel sweeps from their shared bond b_i of the previous sweep to opposite directions, and DMRG steps are performed independently on their own regions, as in the strategy with fixed boundaries. Because of unbalanced initial partitioning, one node usually arrives the shared bond b_i earlier than its neighboring node. Whenever this happens, we allow the faster node going on with its current sweep procedure, until both nodes arrive at a new shared bond $b_{i'}$. The procedure of merging and communication is similar. A global optimized global wave function is obtained by diagonalizing the Hamiltonian in the basis $|\tilde{\alpha}_{i'-1}\rangle^{l}|\sigma_{i'}\rangle|\sigma_{i'+1}\rangle|\tilde{\alpha}_{i'+1}\rangle^{r}$, and on each node the next parallel sweep starts from this new shared bond independently.

Compared to the fixed boundary parallel strategy, there is no waiting time between nodes with adaptive boundaries, as shown in Fig. 1(c). This can greatly reduce load imbalance and improve parallel efficiency. In particular, we have a nearly ideal speedup with 2 nodes even if the initial partitioning is not very good. In the new strategy there are communications between nodes in each DMRG step, by sending real-space position information to its neighbor. However, the time cost of this extra communication is literally negligible.

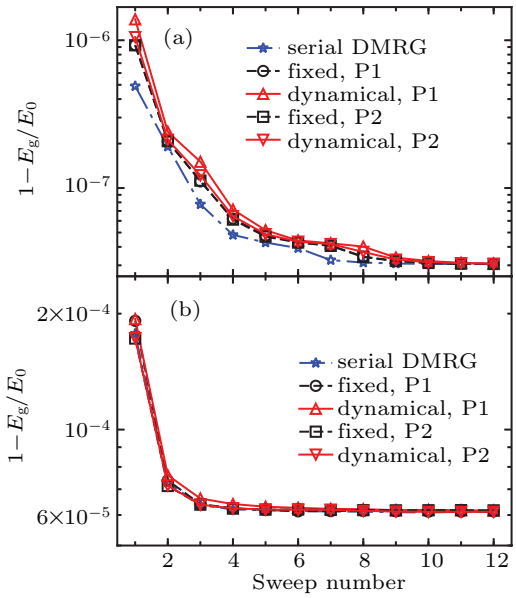

Fig. 2. The energies of two benchmark models after each sweep for the serial DMRG and real-space parallel DMRG with 2 nodes. E_0 is the benchmark energy come from the calculation of other DMRG packages with more kept states. (a) Results for spin-cluster chain in comparison with the convergent ground energy with 6148 states in Itensor.[54] (b) Results for our QCDMRG calculations in comparison with CheMPS2[55] with 2000 $SU(2)$ kept states. The number of kept states and partitionings are set as in Tables 1 and 2, respectively.

Although the initial partitioning hardly affects the parallel efficiency in our scheme, it may give slightly worse results compared to the original strategy for the same number of sweeps, because the environment of the previous sweep is used in DMRG steps across the shared bond. To get high accurate results as the original parallel DMRG, for models with

the reflection symmetry, the preferred initial region size satisfies $L_j = L_{N-j-1}$, where N is number of regions and L_j is the length of the jth region, and $0 \le j < N$. Furthermore, we set a threshold to restrict the boundary shifting between two adjacent sweeps. In our calculations, the position of shared bonds between two nearest sweeps satisfies $|i - i'|/L \le 0.05$ for 2 nodes, where i (i') is the position of the dynamical shared bond in the previous (current) sweep [see Fig. 1(c)] and L is the length of the chain. We test the convergence of our strategy by applying it to two benchmark models (see Fig. 2). With the convergence of the ground state, both fixed and dynamical parallel strategies with different initial partitionings get nearly the same energy as the serial DMRG after the same number of sweeps.

An initial guessing wavefunction at the shared bond is more complicated for the dynamical parallel case. Specifically, it depends on wave functions when two nodes arrive at $b_{i'}$, DMRG steps at the shared bond $b_{i'}$ of the previous half-sweep and the previous sweep. Without loss of generality, we consider the case $i < i'$, in which the shared bond moves to right comparing to the last sweep, as shown in Fig. 1(c). First, from sweeps on the left and right region, one obtains two wavefunctions

$$|\tilde{\Psi}^{i'}\rangle = \sum_{\tilde{\alpha}_{i'-1}\sigma_{i'}\alpha_{i'}} \tilde{\psi}^{\sigma_{i'}}_{\tilde{\alpha}_{i'-1}\alpha_{i'}} |\tilde{\alpha}_{i'-1}\rangle^l |\sigma_{i'}\rangle |\alpha_{i'}\rangle^r, \quad (10)$$

$$|\tilde{\Psi}^{i'+1}\rangle = \sum_{\hat{\alpha}_{i'}\sigma_{i'+1}\tilde{\alpha}_{i'+1}} \tilde{\psi}^{\sigma_{i'+1}}_{\hat{\alpha}_{i'}\tilde{\alpha}_{i'+1}} |\hat{\alpha}_{i'}\rangle^l |\sigma_{i'+1}\rangle |\tilde{\alpha}_{i'+1}\rangle^r, \quad (11)$$

when two nodes arrive at $b_{i'}$. Hereafter a symbol with a hat refers to the previous half-sweep. One may notice that we can not directly get a guessing solution

$$|\Phi^{i',i'+1}\rangle = \sum_{\tilde{\alpha}_{i'-1}\sigma_{i'}\sigma_{i'+1}\tilde{\alpha}_{i'+1}} \phi^{\sigma_{i'}\sigma_{i'+1}}_{\tilde{\alpha}_{i'-1}\tilde{\alpha}_{i'}} |\tilde{\alpha}_{i'-1}\rangle^l |\sigma_{i'}\rangle |\sigma_{i'+1}\rangle |\tilde{\alpha}_{i'+1}\rangle^r \quad (12)$$

similar to Eq. (9). Instead, an extra transformation between basis $|\hat{\alpha}_{i'}\rangle$ and $|\alpha_{i'}\rangle$ is necessary. One can establish the projection $T_{\alpha_{i'},\hat{\alpha}_{i'}}$ by SVD results of the eigenvector at bond $b_{i'}$ in the previous sweep and the previous half-sweep as

$$T_{\alpha_{i'},\hat{\alpha}_{i'}} = (V^{i'\dagger}\hat{V}^{i'})_{\alpha_{i'},\hat{\alpha}_{i'}}. \quad (13)$$

Then we can get $\sum_{\tilde{\alpha}_{i'-1}\sigma_{i'}\hat{\alpha}_{i'}} (\tilde{\psi}^{\sigma_{i'}} T)_{\tilde{\alpha}_{i'-1}\hat{\alpha}_{i'}} |\tilde{\alpha}_{i'-1}\rangle^l |\sigma_{i'}\rangle |\hat{\alpha}_{i'}\rangle^r$ as a good approximation of $|\tilde{\Psi}^{i'}\rangle$. Lastly, we obtain the guessing wave function $|\Phi^{i',i'+1}\rangle$ with its coefficients

$$\phi^{\sigma_{i'}\sigma_{i'+1}} = \tilde{\psi}^{\sigma_{i'}} TC \tilde{\psi}^{\sigma_{i'+1}}, \quad (14)$$

where C is a diagonal matrix with $C_{\hat{\alpha}_{i'}\hat{\alpha}_{i'}} = (\hat{\Lambda}^{i'}_{\hat{\alpha}_{i'}})^{-1}$. For the case $i > i'$, we have the similar wavefunction transformation procedure with projection

$$T_{\alpha_{i'},\hat{\alpha}_{i'}} = (U^{i'\dagger}\hat{U}^{i'})_{\alpha_{i'},\hat{\alpha}_{i'}}$$

and $|\Phi^{i',i'+1}\rangle$ of coefficients

$$\phi^{\sigma_{i'}\sigma_{i'+1}} = \tilde{\psi}^{\sigma_{i'}} C T^{\dagger} \tilde{\psi}^{\sigma_{i'+1}}.$$

In particular, if $i = i'$ for all sweeps, our strategy gets the same initial wave function on the shared bond as the original fixed boundary parallel strategy, and the guessing wavefunction degenerates to the fixed one.

In Fig. 3, we compare the predicted wave function with the optimized wavefunction obtained by diagonalizing the Hamiltonian. The initial wave function is not very good in first several sweeps for both fixed and dynamical boundary parallel strategies, since kept states change dramatically in these sweeps. As approaching to the convergence of the ground state, both the strategies provide better initial wave functions. For the inhomogeneous quantum chemical Hamiltonian, truncation error is site dependent. In the dynamical parallel algorithm, adaptive shared bonds appear at positions where the truncation error is larger, thus this results in larger discrepancy between the predicted and optimized wavefunctions at these bonds.

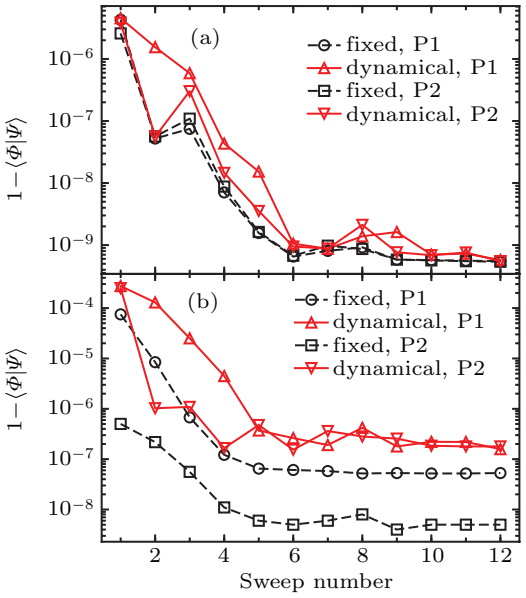

Fig. 3. The distance between the predicted state $|\Phi\rangle$ and the optimized state $|\Psi\rangle$ on the shared bond of each sweep in real-space parallel DMRG with 2 nodes, defined as $1 - \langle\Phi|\Psi\rangle$. (a) Results for the spin-cluster chain. (b) Results for QCDMRG calculations. The number of kept states and partitionings are set as in Tables 1 and 2, respectively.

5. Performance benchmarks

In this section we test the performance of our strategy by applying it to benchmark models in Section 2. Parallel sweeps start after the inifinite-system DMRG,[1,2] and the parallel sweeping pattern for multiple nodes as Ref. [39] is implemented. To reduce the memory and time cost, the number of particles and the z-projection of the total spin are fixed, and the dynamical block state selection approach[28] is used to control the number of kept states in each DMRG step. Specifically, the number of kept states D changes dynamically to keep

the truncation error ε smaller than a tolerance threshold $\varepsilon_{\max}$, within the range $[D_{\min}, D_{\max}]$. Note that truncation error can be larger than $\varepsilon_{\max}$ to keep D smaller than $D_{\max}$. These values for both the benchmark models are shown in Table 1. We perform 12 DMRG sweeps to get convergent ground states. To compare the performances from different initial partitionings, two partitionings are tested for both the models, and note that partitionings for 4 nodes are obtained by dividing regions of partitioning P1 for 2 nodes (see Table 2).

Table 1. Parameters for controlling the number of kept state of each DMRG step in calculations of two benchmark models.

Parameters	SCC	H_2O
$D_{\min}$	512	256
$D_{\max}$	4096	512
$\varepsilon_{\max}$	1e-9	1e-7

Table 2. Initial partitionings for different schemes and different number of nodes.

Model	Partitioning 1 (P1)	Partitioning 2 (P2)
SCC	80,80	70,90
	50,30,30,50	46,34,34,46
H_2O	25,46	35,36
	12,13,16,30	15,10,20,26

The ground state of the spin-cluster chain of periodic boundary condition is calculated with 160 sites and $n_c = 4$. The speedup is defined as the ratio of the time cost for serial DMRG sweeps to that for parallel DMRG sweeps, and the parallel efficiency is the ratio of the speedup to the number of nodes. The speedup of our parallel strategy is shown in Fig. 4(a). For calculations with 2 nodes, the waiting time can almost be ignored for partitioning P1 with equal region size, and we get high parallel efficiency for both parallel strategies. For a bad initial partitioning P2, the speedup of fixed boundary is lower but the dynamical version still has the same high speedup as P1. In 4 nodes, our strategy also shows much higher speedups than the strategy with fixed boundaries and is nearly independent of partitionings. The waiting time is greatly reduced with dynamical boundaries in calculations of the spin-cluster chain. The maximum parallel efficiency is up to 91%.

For the water molecule, we choose the cc-pcVTZ basis to contain 71 molecular orbitals. In the QCDMRG method, a good order of molecular orbitals is useful to avoid local minimal optimizations and may help to fasten the convergence. There are many strategies to optimize the order of molecular orbitals.[56–58] In our calculations, all orbitals are in the order of increasing HF orbital energies. We show speedups of fixed and dynamical parallel DMRG strategies in Fig. 4(b). Similar to calculations for the spin-chain ladder, parallel speedups of our strategy are much higher than the original parallel strategy with fixed boundaries and are almost independent of initial partitionings. Best parallel efficiencies of the water molecule are 88% and 76% for 2 and 4 nodes, respectively. For such short lattice without translational invariant symmetry, few DMRG steps with a large number of kept states take most of the computational time in a whole sweep. Since the maximum waiting time in real-space parallel DMRG is the time cost of a single DMRG step, in general the parallel efficiency in quantum chemical Hamiltonians with small number of orbitals is lower than lattice models. For more complicated quantum chemical systems with larger number of orbitals, our dynamical parallel strategy is expected to have better performance.

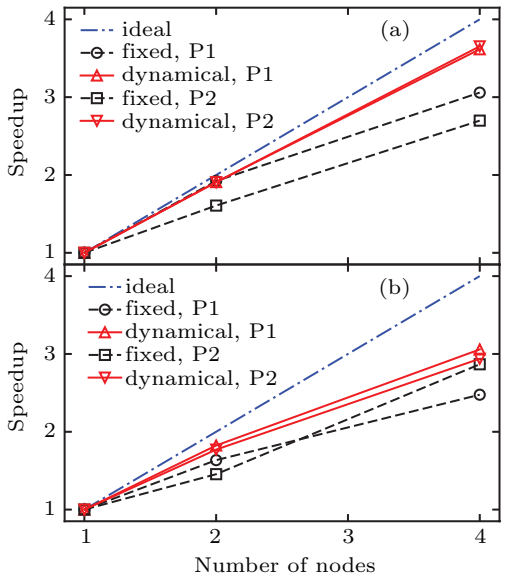

Fig. 4. The speedup for both the fixed and dynamic boundary strategies in calculations of (a) the ground state of the spin-cluster chain, and (b) the QCDMRG method.

6. Conclusions

In summary, we have proposed an improved real-space parallel DMRG strategy with dynamical boundaries, where the waiting time between two nearest nodes is greatly reduced. To get high parallel efficiency, a good initial wave function for the DMRG step on the shared bond is also provided. We test the performance of our parallel strategy in computing the ground state of the spin-cluster chain and the Hamiltonian in quantum chemistry. Compared with the original fixed boundary parallel scheme, our strategy shows higher parallel efficiencies for both the systems, and gets almost the same speedup for different initial partitionings. This real-space parallel strategy can be applied to speed up DMRG calculations with heavy computations, and is easy to be extended to other real-space parallel applications generalized from DMRG, such as various time-dependent algorithms.[59,60]

References

[1] White S R 1992 *Phys. Rev. Lett.* **69** 2863
[2] White S R 1993 *Phys. Rev. B* **48** 10345
[3] Verstraete F, Porras D and Cirac J I 2004 *Phys. Rev. Lett.* **93** 227205
[4] Schollwöck U 2011 *Ann. Phys.* **326** 96

[5] Cheng C, Mao B B, Chen F Z and Luo H G 2015 *Europhys. Lett.* **110** 37002
[6] Cheng C, Mao B B, Chen F Z and Luo H G 2015 *Eur. Phys. J. B* **88** 152
[7] Bravo B, Cabra D C, Gómez Albarracín F A and Rossini G L 2017 *Phys. Rev. B* **96** 054441
[8] Dür W, Hartmann L, Hein M, Lewenstein M and Briegel H J 2005 *Phys. Rev. Lett.* **94** 097203
[9] White S R and Scalapino D J 2003 *Phys. Rev. Lett.* **91** 136403
[10] Ramos F B and Xavier J C 2014 *Phys. Rev. B* **89** 094424
[11] Cheng C, Mondaini R and Rigol M 2018 *Phys. Rev. B* **98** 121112
[12] White S R and Chernyshev A L 2007 *Phys. Rev. Lett.* **99** 127004
[13] Depenbrock S, McCulloch I P and Schollwöck U 2012 *Phys. Rev. Lett.* **109** 067201
[14] Stoudenmire E M and White S R 2012 *Ann. Rev. Condens. Matter Phys.* **3** 111
[15] Zheng B X, Chung C M, Corboz P, Ehlers G, Qin M P, Noack R M, Shi H, White S R, Zhang S and Chan G K L 2017 *Science* **358** 1155
[16] Wang L and Sandvik A W 2018 *Phys. Rev. Lett.* **121** 107202
[17] Yu W C, Cheng C and Sacramento P D 2020 *Phys. Rev. B* **101** 245131
[18] Xiang T 1996 *Phys. Rev. B* **53** R10445
[19] Motruk J, Zaletel M P, Mong R S K and Pollmann F 2016 *Phys. Rev. B* **93** 155139
[20] Ehlers G, White S R and Noack R M 2017 *Phys. Rev. B* **95** 125125
[21] White S R and Martin R L 1999 *J. Chem. Phys.* **110** 4127
[22] Chan G K L and Sharma S 2011 *Ann. Rev. Phys. Chem.* **62** 465
[23] Baiardi A and Reiher M 2020 *J. Chem. Phys.* **152** 040903
[24] Luo H G, Qin M P and Xiang T 2010 *Phys. Rev. B* **81** 235129
[25] Alvarez G 2010 *Comput. Phys. Commun.* **180** 1572
[26] Tzeng Y C 2012 *Phys. Rev. B* **86** 024403
[27] White S R 1996 *Phys. Rev. Lett.* **77** 3633
[28] Legeza O, Röder J and Hess B A 2003 *Phys. Rev. B* **67** 125114
[29] Legeza O and Sólyom J 2003 *Phys. Rev. B* **68** 195116
[30] White S R 2005 *Phys. Rev. B* **72** 180403
[31] Hubig C, McCulloch I P, Schollwöck U and Wolf F A 2015 *Phys. Rev. B* **91** 155115
[32] Núñez Fernández Y and Torroba G 2020 *Phys. Rev. B* **101** 085135
[33] Kurashige Y and Yanai T 2009 *J. Chem. Phys.* **130** 234114
[34] Chan G K L 2004 *J. Chem. Phys.* **120** 3172
[35] Hager G, Jeckelmann E, Fehske H and Wellein G 2004 *J. Comput. Phys.* **194** 795
[36] Nemes C, Barcza G, Nagy Z, Legeza O and Szolgay P 2014 *Comput. Phys. Commun.* **185** 1570
[37] Chen F Z, Cheng C and Luo H G 2019 *Acta Phys. Sin.* **68** 120202 (in Chinese)
[38] Chen F Z, Cheng C and Luo H G 2020 *Chin. Phys. B* **29** 070202
[39] Stoudenmire E M and White S R 2013 *Phys. Rev. B* **87** 155137
[40] Ueda H 2018 *J. Phys. Soc. Jpn.* **87** 074005
[41] Urbanek M and Soldán P 2016 *Comput. Phys. Commun.* **199** 170
[42] Secular P, Gourianov N, Lubasch M, Dolgov S, Clark S R and Jaksch D 2020 *Phys. Rev. B* **101** 235123
[43] Starova G L, Filatov S K, Fundamensky V S and Vergasova L P 1991 *Mineralog. Mag.* **55** 613
[44] Fujihala M, Sugimoto T, Tohyama T, Mitsuda S, Mole R A, Yu D H, Yano S, Inagaki Y, Morodomi H, Kawae T, Sagayama H, Kumai R, Murakami Y, Tomiyasu K, Matsuo A and Kindo K 2018 *Phys. Rev. Lett.* **120** 077201
[45] Hase M, Rule K C, Hester J R, Fernandez-Baca J A, Masuda T and Matsuo Y 2019 *J. Phys. Soc. Jpn.* **88** 094708
[46] Zhou Z, Chen F, Zhong Y, Luo H G and Zhao J 2019 *Phys. Rev. B* **99** 205143
[47] Furrer A, Podlesnyak A, Clemente-Juan J M, Pomjakushina E and Güdel H U 2020 *Phys. Rev. B* **101** 224417
[48] Chan G K L and Head-Gordon M 2003 *J. Chem. Phys.* **118** 8551
[49] Hachmann J, Cardoen W and Chan G K L 2006 *J. Chem. Phys.* **125** 144101
[50] Marti K H, Ondík I M, Moritz G and Reiher M 2008 *J. Chem. Phys.* **128** 014104
[51] Sharma S, Sivalingam K, Neese F and Chan G K L 2014 *Nat. Chem.* **6** 927
[52] Knecht S, Legeza O and Reiher M 2014 *J. Chem. Phys.* **140** 041101
[53] Smith D G A, Burns L A, Simmonett A C, Parrish R M, Schieber M C, Galvelis R, Kraus P, Kruse H, Di Remigio R, Alenaizan A, James A M, Lehtola S, Misiewicz J P, Scheurer M, Shaw R A, Schriber J B, Xie Y, Glick Z L, Sirianni D A, O'Brien J S, Waldrop J M, Kumar A, Hohenstein E G, Pritchard B P, Brooks B R, Schaefer H F, Sokolov A Y, Patkowski K, DePrince A E, Bozkaya U, King R A, Evangelista F A, Turney J M, Crawford T D and Sherrill C D 2020 *J. Chem. Phys.* **152** 184108
[54] Fishman M, White S R and Miles Stoudenmire E 2020 arXiv:2007.14822 [cs.MS]
[55] Wouters S, Poelmans W, Ayers P W and Neck D V 2014 *Comput. Phys. Commun.* **185** 1501
[56] Chan G K L and Head-Gordon M 2002 *J. Chem. Phys.* **116** 4462
[57] Moritz G, Hess B A and Reiher M 2005 *J. Chem. Phys.* **122** 024107
[58] Rissler J, Noack R M and White S R 2006 *Chem. Phys.* **323** 519
[59] White S R and Feiguin A E 2004 *Phys. Rev. Lett.* **93** 076401
[60] Haegeman J, Cirac J I, Osborne T J, Pižorn I, Verschelde H and Verstraete F 2011 *Phys. Rev. Lett.* **107** 070601